Color tuning associated with heteroleptic cyclometalated Ir(III) complexes: influence of the ancillary ligand†

Chau-Jiun Chang,[a] Cheng-Han Yang,[a] Kellen Chen,[a] Yun Chi,*[a] Ching-Fong Shu,*[b] Mei-Lin Ho,[c] Yu-Shan Yeh[c] and Pi-Tai Chou*[c]

Received 22nd January 2007, Accepted 28th February 2007
First published as an Advance Article on the web 23rd March 2007
DOI: 10.1039/b700998d

We report the preparation of a series of new heteroleptic Ir(III) metal complexes chelated by two cyclometalated 1-(2,4-difluorophenyl)pyrazole ligands (dfpz)H and a third ancillary bidentate ligand (L^X). Such an intricate design lies in a core concept that the cyclometalated dfpz ligands always warrant a greater ππ* gap in these series of iridium complexes. Accordingly, the lowest one-electron excitation would accommodate the π* orbital of the ancillary L^X ligands, the functionalization of which is then exploited to fine-tune the phosphorescent emission wavelengths. Amongst the L^X ligands designed, three classes (series **1**–**3**) can be categorized, and remarkable bathochromic shifts of phosphorescence were observed by (i) replacing the 2-benzoxazol-2-yl substituent (**1a**) with the 2-benzothiazol-2-yl group (**1b**) in the phenolate complexes, (ii) converting the pyridyl group (**2a**) to the pyrazolyl group (**2b**) and even to the isoquinolyl group (**2c**) in the pyrazolate complexes and (iii) extending the π-conjugation of the benzimidazolate ligand from **3a** to **3b**. Single-crystal X-ray diffraction study on complex [(dfpz)Ir(bzpz)] (**2b**) was conducted to confirm their general molecular architectures. Complex **2b** was also used as a representative example for fabrication of multilayered, green-emitting phosphorescent OLEDs using the direct thermal evaporation technique.

Introduction

Organometallic complexes involving third-row transition metal elements have become crucial for the fabrication of highly efficient organic light emitting diodes (OLEDs).[1] The strong spin–orbit coupling induced by a heavy metal ion such as iridium(III) promotes an efficient intersystem crossing from the singlet to the triplet excited state manifold, which then facilitates strong electroluminescence by harnessing both singlet and triplet excitons after the initial charge recombination. Because internal phosphorescence quantum efficiency (η_{int}) as high as ~100% can theoretically be achieved, these heavy metal containing emitters will be superior to their fluorescent counterparts in future OLED applications.[2] As a result, there is a continuous trend of shifting research focusing on these heavy transition metal complexes.

Moreover, since the manufacture of a full color display requires the use of emitters with all three primary colors, *i.e.* blue, green and red, rationally tuning emission color over the entire visible range has emerged as an important task.[3] Several precedents involving the third-row metal elements were documented; for example: by choosing appropriate σ-alkynyl ligands with different degrees of π-conjugation, the emission of the multi-functionalized or the tridentate cyclometalating Pt(II) complexes can be systematically varied from green-yellow to saturated red.[4] Moreover, homoleptic azolate complexes [Pt(N^N)$_2$], N^NH = 2-pyridyl azole, were reported to exhibit tunable and highly efficient phosphorescence.[5] On the other hand, varying the ancillary ligands from carbonyl to phosphine or pyridine donors in the octahedral pyridyl azolate Os(II) system led to a significant lowering of the ^{3}MLCT energy gap, giving a notable change from blue to green and then to saturated red and near infrared (NIR) emission.[6]

For the related Ir(III) complexes, the systematic derivatization of cyclometalated ligands has also allowed a lucid prediction of their emission colors.[7] It has been documented that the LUMO and HOMO of the homoleptic, tris-cyclometalated complexes [Ir(ppy)$_3$], ppy = 2-phenylpyridine, are mainly located at the pyridyl segment of the ppy ligands and the phenyl and central metal d_π segments, respectively.[8] Accordingly, addition of electron withdrawing (or releasing) groups at the pyridyl site would display a significant decrease (or increase) of the LUMO energy level. Conversely, the addition of electron withdrawing (donating) substituents at the phenyl group would stabilize (destabilize) the HOMO energy level.[9] Thus, even without the assistance of theoretical computation, such an energy tuning strategy can qualitatively predict the phosphorescent wavelengths within a series of functionalized complexes.

In yet another approach, the emission of the heteroleptic complexes [Ir(C^N)$_2$(L^X)], such as [Ir(ppy)$_2$(L^X)] and [Ir(piq)$_2$(L^X)], (piq)H = 1-phenylisoquinoline, could be tuned by varying the third, ancillary ligand (L^X), among which the bidentate chelating anions such as acetylacetonate, picolinate, *N*-methylsalicylimine, pyrazolate and even pyrazolyl borate have been exploited.[10] It is notable, however, that the resulting

[a]*Department of Chemistry, National Tsing Hua University, Hsinchu 300, Taiwan. E-mail: ychi@mx.nthu.edu.tw; Fax: +886-3-772-0864; Tel: +886-2-571-2956*
[b]*Department of Applied Chemistry, National Chiao Tung University, Hsinchu 300, Taiwan. E-mail: shu@cc.nctu.edu.tw; Fax: +886-3-572-3764; Tel: +886-3-571-2121 ext. 56544*
[c]*Department of Chemistry, National Taiwan University, Taipei 106, Taiwan. E-mail: chop@ntu.edu.tw; Fax: +886-2-23695208; Tel: +886-2-33663894*
† The HTML version of this article has been enhanced with colour images.

phosphorescence wavelength of these complexes was largely governed by the pair of orthogonal cyclometalating C^N ligands, while the third L^X ligand had only a secondary and relatively smaller influence. Obviously, this is due to the fact that most of the L^X ligands possess a significantly larger ππ* energy gap and, thus, they tend to affect solely the metal d_π orbitals contributing to the HOMO through their inherent electron withdrawing (or donating) properties.[11]

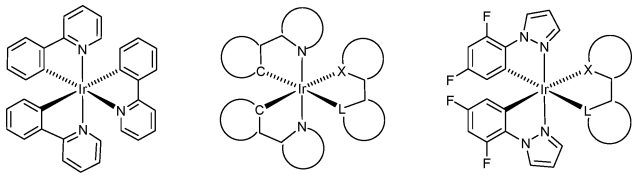

In this paper, we report the synthesis and characterization of a series of a new class of heteroleptic iridium complexes with formula [Ir(dfpz)$_2$(L^X)], dfpzH = 1-(2,4-difluorophenyl)pyrazole. In contrast to the previously reported [Ir(ppy)$_2$(L^X)] and [Ir(piq)$_2$(L^X)] systems,[12] the exceedingly large ππ* energy gap of the dfpz ligands in these Ir(III) complexes[13] allowed the third, ancillary L^X ligand to dominate the lowest lying excited state. As a result, tuning the emission color among these complexes can be achieved by systematically employing various distinctive L^X ligands, simplifying the design strategy and hence the synthetic task. Our designs are somewhat analogous to those of the Ir(III) complexes with phenylpyrazole (ppz) and neutral diimine ligands[14] and even the isoquinolinecarboxylate ligand as the tunable phosphors.[15] As for the second example, due to the smaller energy gap of cyclometalated ppz ligands, its alkyl substituents can still exert a weak influence over the final emission color according to experimental work and the accompanying DFT calculations.

Experimental

General information and materials

All reactions were performed under a nitrogen atmosphere using anhydrous solvents or solvents treated with an appropriate drying reagent. Mass spectra were obtained on a JEOL SX-102A instrument operating in electron impact (EI) mode or fast atom bombardment (FAB) mode. ^{1}H and ^{19}F NMR spectra were recorded on Varian Mercury-400 or INOVA-500 instruments. Elemental analyses were conducted at the NSC Regional Instrumentation Center at National Chiao Tung University. The chelating azolate ligands: 3-*tert*-butyl-5-(2-pyridyl)pyrazole (bppzH), 3-*tert*-butyl-5-(2-pyrazyl)pyrazole (bzpzH), 3-*tert*-butyl-5-(2-isoquinolyl)pyrazole (bqpzH) and 3-trifluoromethyl-5-(2-pyridyl) pyrazole (fppzH), were prepared according to the literature procedures,[16] while 1-(2,4-difluorophenyl)pyrazole (dfpzH) was prepared from reaction of 2,4-difluorophenyl hydrazine hydrochloride with 1,1,3,3-tetramethoxypropane, and was directly used for the preparation of chloride-bridged dimer [(dfpz)$_2$IrCl]$_2$ according to the literature.[13,17] The imidazole ligands, namely: 2-(2-quinolinyl)benzimidazole (qbimH) was obtained from condensation of quinoline-2-carboxylic acid with 1,2-phenylenediamine;[18] while other bidentate ligands: 2-(2-pyridyl)benzimidazole (pbimH), 2-benzoxazol-2-yl phenol (bopH) and 2-benzothiazol-2-yl phenol (btpH) were purchased from Aldrich Chem. Inc.

Syntheses

Synthesis of [(dfpz)$_2$Ir(bop)] (1a). A mixture of [(dfpz)$_2$IrCl]$_2$ (100 mg, 0.085 mmol), 2-benzoxazol-2-yl phenol (bopH, 50 mg, 0.21 mmol), and Na_2CO_3 (90 mg, 0.85 mmol) in 2-methoxyethanol (25 mL) was heated to reflux for 4 h. An excess of water was added after the solution was cooled to RT (room temperature). The precipitate was collected by filtration and washed with ethanol (10 mL), followed by diethyl ether (10 mL). Yellowish green [(dfpz)$_2$Ir(bop)] (**1a**) was obtained from column chromatography using ethyl acetate and hexane (1 : 2) as eluent, followed by recrystallization from CH_2Cl_2 and hexane at room temperature; yield: 100 mg, 0.13 mmol, 73%.

The orange benzothiazolyl complex [(dfpz)$_2$Ir(btp)] (**1b**) was prepared using a similar procedure, yield: 76%.

Spectral data for ***1a****.* MS (FAB, ^{193}Ir), *m*/*z*: 762 [M$^+$ + 1]. ^{1}H NMR (400 MHz, d$_6$-acetone, 298 K): δ 8.56 (d, 1H, J_{HH} = 2.8 Hz), 8.46 (d, 1H, J_{HH} = 2.8 Hz), 7.92 (dd, 1H, J_{HH} = 8.0, 1.0 Hz), 7.70 (d, 1H, J_{HH} = 2.4 Hz), 7.63–7.58 (m, 2H), 7.29 (t, 1H, J_{HH} = 8.0 Hz), 7.20 (ddd, 1H, J_{HH} = 5.2, 5.2, 1.6 Hz), 7.06 (t, 1H, J_{HH} = 8.0 Hz), 6.77–6.66 (m, 5H), 6.61 (d, 1H, J_{HH} = 8.4 Hz), 6.49 (t, 1H, J_{HH} = 6.6 Hz), 5.91 (dd, 1H, J_{HH} = 8.4, 2.4 Hz), 8.56 (dd, 1H, J_{HH} = 8.4, 2.4 Hz). ^{19}F NMR (470 MHz, d$_6$-acetone, 298 K): δ −114.33 (1F), −114.34 (1F), −124.68 (1F), −125.80 (1F). Anal. Calcd for $C_{31}H_{18}F_4IrN_5O_2$: C, 48.94; H, 2.38; N, 9.21. Found: C, 48.51; H, 2.64: N, 9.19%.

Spectral data for ***1b****.* MS (FAB, ^{193}Ir), *m*/*z*: 777 [M$^+$ + 1]. ^{1}H NMR (400 MHz, d$_6$-acetone, 298 K): δ 8.60 (d, 1H, J_{HH} = 2.8 Hz), 8.39 (d, 1H, J_{HH} = 2.8 Hz), 7.97 (d, 1H, J_{HH} = 0.8 Hz), 7.95 (d, 1H, JHH = 0.8 Hz), 7.61–7.58 (m, 2H), 7.34–7.20 (m, 4H), 6.78 (t, 1H, J_{HH} = 2.4 Hz), 6.71 (t, 1H, J_{HH} = 2.4 Hz), 6.70–6.53 (m, 4H), 6.03 (dd, 1H, J_{HH} = 8.8, 2.4 Hz), 5.42 (dd, 1H, J_{HH} = 8.8, 2.4 Hz). ^{19}F NMR (470 MHz, d$_6$-acetone, 298 K): δ −114.67 (1F), −114.82 (1F), −124.94 (1F), −125.65 (1F). Anal. Calcd for $C_{31}H_{18}F_4IrN_5OS$: C, 47.93; H, 2.34; N, 9.02. Found: C, 48.06; H, 2.59: N, 8.99%.

Synthesis of [(dfpz)$_2$Ir(bppz)] (2a). A mixture of [(dfpz)$_2$IrCl]$_2$ (100 mg, 0.09 mmol), 3-*tert*-butyl-5-(2-pyridyl) pyrazole (bppzH, 40 mg, 0.21 mmol), and Na_2CO_3 (90 mg, 0.85 mmol) in 2-methoxyethanol (20 mL) was heated to reflux for 4 h. An excess of water was added after the solution was cooled to RT (room temperature). The precipitate was collected by filtration and washed with ethanol (10 mL), followed by diethyl ether (10 mL). Pure samples of [(dfpz)$_2$Ir(bppz)] (**2a**) were obtained from column chromatography using ethyl acetate and hexane as eluent, followed by recrystallization from CH_2Cl_2 and hexane at room temperature; yield: 90 mg, 0.12 mmol, 70%. The related complexes [(dfpz)$_2$Ir(bzpz)] (**2b**), [(dfpz)$_2$Ir(bqpz)] (**2c**) and [(dfpz)$_2$Ir(fppz)] (**2d**) were prepared using similar procedures, yield: 65–70%.

Spectral data for ***2a****.* MS (FAB, ^{193}Ir), *m*/*z*: 752 [M$^+$ + 1]. ^{1}H NMR (400 MHz, $CDCl_3$, 298 K): δ 8.29 (d, 1H, J_{HH} = 2.8 Hz), 8.22 (d, 1H, J_{HH} = 3.2 Hz), 7.82 (d, 1H, J_{HH} = 5.6 Hz), 7.68–7.65 (m, 2H), 6.92 (s, 1H), 6.81 (d, 1H, J_{HH} = 2.0 Hz), 6.65 (s, 1H), 6.57–6.50 (m, 3H), 6.45–6.42 (m, 2H), 5.76 (dd, 1H, J_{HH} = 8.0, 2.4 Hz), 5.70 (dd, 1H, J_{HH} = 8.0, 2.4 Hz), 1.31 (s, 9H). ^{19}F

NMR (470 MHz, d_6-acetone, 298 K): δ −113.80 (1F), −115.39 (1F), −124.91 (1F), −126.37 (1F). Anal. Calcd for $C_{30}H_{24}F_4IrN_7$: C, 47.99; H, 3.22; N, 13.06. Found: C, 47.56; H, 3.62: N, 12.98%.

Spectral data for ***2b****.* MS (FAB, ^{193}Ir), *m/z*: 754 [M^+ + 1]. ^{1}H NMR (400 MHz, d_6-acetone, 298 K): δ 9.13 (s, 1H), 8.50 (d, 2H, J_{HH} = 16.0 Hz), 8.21 (d, 1H, J_{HH} = 3.6 Hz), 7.91 (d, 1H, J_{HH} = 3.6 Hz), 7.40 (s, 1H), 6.79–6.65 (m, 6H), 5.87 (d, 1H, J_{HH} = 8.4 Hz), 5.71 (d, 1H, J_{HH} = 8.4 Hz), 1.31 (s, 9H). Anal. Calcd for $C_{29}H_{23}F_4IrN_8$: C, 46.33; H, 3.08; N, 14.91. Found: C, 46.44; H, 3.56: N, 14.95%.

Spectral data for ***2c****.* MS (FAB, ^{193}Ir), *m/z*: 802 [M^+ + 1]. ^{1}H NMR (400 MHz, d_6-acetone, 298 K): δ 9.02 (d, 1H, J_{HH} = 7.5 Hz), 8.49 (d, 1H, J_{HH} = 3.0 Hz), 8.45 (d, 1H, J_{HH} = 3.0 Hz), 7.96 (dd, 1H, J_{HH} = 7.0, 2.5 Hz), 7.92 (d, 1H, J_{HH} = 10.5 Hz), 7.85–7.80 (m, 2H), 7.50 (d, 1H, J_{HH} = 3.0 Hz), 7.12 (d, 1H, JHH = 2.0 Hz), 7.11 (s, 1H), 6.79–6.74 (m, 1H), 6.68–6.62 (m, 3H), 6.57 (d, 1H, J_{HH} = 2.0 Hz), 5.90 (dd, 1H, J_{HH} = 8.3, 2.3 Hz), 5.77 (dd, 1H, J_{HH} = 8.3, 2.3Hz). ^{19}F NMR (470 MHz, d_6-acetone, 298 K): δ −113.90 (1F), −115.41 (1F), −124.85 (1F), −126.42 (1F). Anal. Calcd for $C_{34}H_{26}F_4IrN_7$: C, 50.99; H, 3.27; N, 12.24. Found: C, 50.94; H, 3.67: N, 12.14%.

Spectral data for ***2d****.* MS (FAB), *m/z*: 764 [M^+]. ^{1}H NMR (500 MHz, $CDCl_3$, 294 K): δ 8.23 (dd, J_{HF} = 16.3, 3.5 Hz, 2H), 7.87 (d, J_{HH} = 5.5 Hz, 1H), 7.76–7.80 (m, 2H), 7.06 (t, J_{HH} = 5.8 Hz, 1H), 6.96 (s, 1H), 6.86 (d, J_{HH} = 1.5 Hz, 1H), 6.76 (d, J_{HH} = 2.0 Hz, 1H), 6.51–6.44 (m, 4H), 5.76 (dd, J_{HH} = 6.5, 2.5 Hz, 1H), 5.68 (dd, J_{HH} = 8.5, 2.0 Hz, 1H). ^{19}F NMR (470 MHz, $CDCl_3$, 294 K): δ −125.6 (1F), −124.8 (1F), −113.8 (1F), −113.2 (1F), −60.3 (s, 3F). Anal. Calcd for $C_{27}H_{15}F_7IrN_7$: N, 12.86; C, 42.52; H, 1.98. Found: N, 12.89; C, 42.28; H, 2.05%.

Synthesis of [(dfpz)$_2$Ir(pbim)] (3a). A mixture of [(dfpz)$_2$IrCl]$_2$ (200 mg, 0.17 mmol), 2-pyridyl benzimidazole (pbimH, 80 mg, 0.42 mmol), and Na_2CO_3 (180 mg, 1.7 mmol) in 2-methoxyethanol (35 mL) was heated to reflux for 4 h. An excess of water was added after the solution was cooled to RT (room temperature). The precipitate was collected by filtration and washed with ethanol (10 mL), followed by diethyl ether (10 mL). Yellowish green [(dfpz)$_2$Ir(pbim)] (**3a**) was obtained from column chromatography using ethyl acetate as eluent, followed by recrystallization from CH_2Cl_2 and hexane at room temperature; yield: 180 mg, 0.24 mmol, 71%. The related 2-quinolinyl complex [(dfpz)$_2$Ir(qbim)] **3b** was obtained using similar procedures.

Spectral data for ***3a****.* MS (FAB, ^{193}Ir), *m/z*: 746 [M^+ + 1]. ^{1}H NMR (400 MHz d_6-acetone, 298 K): δ 8.53 (d, 1H, J_{HH} = 3.0 Hz), 8.48 (d, 1H, J_{HH} = 3.0 Hz), 8.45 (d, 1H, J_{HH} = 7.0 Hz), 8.08–8.05 (m, 2H), 7.57 (d, 1H, J_{HH} = 8.0 Hz), 7.36 (dd, 1H, J_{HH} = 6.5, 5.3 Hz), 7.20 (d, 1H, J_{HH} = 2.0 Hz), 6.95 (dd, 1H, J_{HH} = 8.5, 6.5 Hz), 6.88–6.80 (m, 3H), 6.72 (dd, 1H, J_{HH} = 7.5, 6.5 Hz), 6.66–6.63 (m, 2H), 6.30 (d, 1H, J_{HH} = 8.5 Hz), 5.96 (dd, 1H, J_{HH} = 7.5, 2.0 Hz), 5.89 (dd, 1H, J_{HH} = 7.5, 2.0 Hz). ^{19}F NMR (470 MHz, d_6-acetone, 298 K): δ −113.78 (1F), −114.49 (1F), −124.60 (1F), −125.29 (1F). Anal. Calcd for $C_{30}H_{18}F_4IrN_7$: C, 48.38; H, 2.44; N, 13.17. Found: C, 48.07; H, 2.66: N, 13.06%.

Spectral data for ***3b****.* MS (FAB, ^{193}Ir), *m/z*: 795 [M^+ + 1]. ^{1}H NMR (400 MHz, $CDCl_3$, 298 K): δ 8.83 (d, 1H, J_{HH} = 8.4 Hz), 8.33–8.32 (m, 2H), 8.22 (d, 1H, J_{HH} = 8.8 Hz), 8.18 (d, 1H, J_{HH} = 3.0 Hz), 7.81 (dd, 2H, J_{HH} = 13.6, 8.4 Hz), 7.44 (t, 1H, J_{HH} = 7.6 Hz), 7.31 (t, 1H, J_{HH} = 8.4 Hz), 7.12 (t, 1H, J_{HH} = 8.0 Hz), 7.00 (d, 1H, J_{HH} = 2.0 Hz), 6.84 (t, 1H, J_{HH} = 8.0 Hz), 6.70 (ddd, 1H, J_{HH} = 11.6, 9.0, 2.6 Hz), 6.57 (ddd, 1H, J_{HH} = 11.6, 9.0, 2.6 Hz), 6.47 (d, 1H, J_{HH} = 2.4 Hz), 6.41 (dd, 1H, J_{HH} = 2.8, 2.4 Hz), 6.29 (dd, 1H, J_{HH} = 2.8, 2.4 Hz), 6.07 (d, 1H, J_{HH} = 8.4 Hz), 5.77 (dd, 1H, J_{HH} = 8.74, 2.8 Hz), 5.62 (dd, 1H, J_{HH} = 8.4, 2.8 Hz). ^{19}F NMR (470 MHz, $CDCl_3$, 298 K): δ −112.29 (2F), −123.57 (1F), −124.25 (1F). Anal. Calcd for $C_{34}H_{20}F_4IrN_7$: C, 51.38; H, 2.54; N, 12.34. Found: C, 51.34; H, 2.96: N, 12.15%.

X-Ray diffraction study

Single crystal X-ray analysis was measured on a Bruker SMART Apex CCD diffractometer using λ(Mo-Kα) radiation (λ = 0.71073 Å). The data collection was executed using the SMART program. Cell refinement and data reduction were made by the SAINT program. The structure was determined using the SHELXTL/PC program and refined using full-matrix least squares. All non-hydrogen atoms were refined anisotropically, whereas hydrogen atoms were placed at the calculated positions and included in the final stage of refinements with fixed parameters. Crystallographic refinement parameters of complex **2b** are summarized in Table 1.

CCDC reference numbers 634398.

For crystallographic data in CIF or other electronic format see DOI: 10.1039/b700998d

Spectral measurement

Steady-state absorption and emission spectra were recorded with a Hitachi (U-3310) spectrophotometer and an Edinburgh (FS920) fluorimeter, respectively. For the emission with peak wavelength <550 nm, quinine sulfate with an emission yield of Φ ~ 0.55 (λ_{max} ~ 460 nm) in 1.0 N H_2SO_4 served as a standard to calculate the emission quantum yield.[19] On the other hand, DCM (4-(dicyanomethylene)-2-methyl-6-(*para*-dimethylaminostyryl)-4*H*-pyran, λ_{max} = 615 nm, Exciton) in methanol, with quantum yield of ~0.43, served as the standard for measuring the quantum yield of the emission band of ≥550 nm.[20] Lifetime studies were performed with an Edinburgh FL 900 photon-counting system with a hydrogen-filled/or a nitrogen

Table 1 X-Ray structural data for complex **2b**

Formula	$C_{29}H_{23}F_4IrN_8$
M	751.75
Crystal system	Monoclinic
Space group	$P2_1/c$
T/K	150(2)
a/Å	10.4704(4)
b/Å	21.4926(8)
c/Å	12.0294(5)
β/°	90.799(1)
V/Å^3	2706.79(18)
Z	4
D_c/g cm^{-3}	1.845
F(000)	1464
μ(Mo-K$_\alpha$)/mm^{-1}	4.996
Crystal size/mm	0.20 × 0.13 × 0.10
h, *k*, *l* ranges	−13 to 13, −27 to 26, −15 to 14
Transmission: max, min.	0.6349, 0.4348
Data/restraints/parameters	6207/0/413
GOF on F^2	1.148
R_1, wR_2 with $I > 2\sigma(I)$	0.0384, 0.0730
D-map, max, min/e Å^{-3}	1.935, −2.128

lamp as the excitation source. Data were analyzed using the nonlinear least squares procedure in combination with an iterative convolution method. The emission decays were analyzed by the sum of exponential functions, which allows partial removal of the instrument time broadening and consequently renders a temporal resolution of ~200 ps.

Computational methodology

Calculations on the electronic ground state of the studied complexes were carried out using B3LYP density functional theory.[21] A "double-ζ" quality basis set consisting of Hay and Wadt's effective core potentials (LANL2DZ)[22] was employed for the Ir atom, and a 6-31G* basis, for H, C, N, F and O atoms. A relativistic effective core potential (ECP) replaced the inner core electrons of Ir(III), leaving the outer core ($5s^2 5p^6$) electrons and the $5d^6$ valence electrons. Time-dependent DFT (TDDFT) calculations using the B3LYP functional were then performed on the basis of the structural optimized geometries. Typically, the lowest 10 triplet and 10 singlet roots of the nonhermitian eigenvalue equations were obtained to determine the vertical excitation energies. Oscillator strengths were deduced from the dipole transition matrix elements (for singlet states only). The ground-state B3LYP and excited-state TDDFT calculations were carried out using Gaussian03.[23]

Electrochemical measurement

Cyclic voltammetry (CV) measurements were performed using a BAS 100 B/W electrochemical analyzer. The oxidation and reduction measurements were recorded using Pt wire and an Au disk coated with Hg as working electrodes, respectively, in anhydrous CH_2Cl_2 and anhydrous THF containing 0.1 M $(TBA)PF_6$ as the supporting electrolyte, at a scan rate of 50 mV s^{-1}. The potentials were measured against an Ag/Ag^+ (0.01 M $AgNO_3$) reference electrode with ferrocene as the internal standard.

Fabrication of OLEDs

Dopant emitter **2b**, in five different concentrations from 7 to 100%, were fabricated for the phosphorescent OLEDs. Our devices have the conventional multilayer configuration: ITO/NPB (40 nm)/**2b** dopant in CBP (30 nm)/BCP(10 nm)/AlQ_3(30 nm)/Mg : Ag (55 nm); where NPB (1,4-bis(1-naphthylphenylamino)biphenyl) served as the hole transport layer, while CBP (4,4′-bis-(9-carbazolyl)biphenyl), BCP (2,9-dimethyl-4,7-diphenyl-1,10-phenanthroline) and AlQ_3 (tris-(8-hydroxyquinolinyl) aluminium) functioned as the host matrix, hole blocking layer and electron transport layer, respectively. The cathode Mg : Ag alloy (10 : 1) was deposited onto the AlQ_3 layer by coevaporation. An additional layer of Ag (100 nm) was deposited onto the cathode as a protective coating. The current–voltage–luminance was measured at ambient conditions with a Keithley 2400 source meter and a Newport 1835C optical meter equipped with an 818ST silicon photodiode.

Results and discussion

Synthesis and characterization

Treatment of the cyclometalating ligands (dfpz)H with $IrCl_3 \cdot nH_2O$ in refluxing ethoxyethanol afforded the respective chloride bridged iridium complex $[(dfpz)_2IrCl]_2$. Three parent heteroleptic iridium complexes, $[(dfpz)_2Ir(bop)]$ (**1a**), $[(dfpz)_2Ir(bppz)]$ (**2a**) and $[(dfpz)_2Ir(pbim)]$ (**3a**), possessing respectively 2-benzothiazol-2-yl phenolate, 2-pyridylpyrazolate and 2-pyridylbenzimidazolate, as well as other functionalized derivatives, were prepared from the direct reaction of $[(dfpz)_2IrCl]_2$ with each of the designated ancillary ligands in the presence of Na_2CO_3 as proton scavenger. Chart 1 summarizes their structural drawings as well as their numbering codes. It is notable that all these iridium complexes are moderately soluble in chlorinated solvents. However, they show good thermal stability, as supported by negligible degradation in the solution phase over a long period of time. Detailed characterizations were carried out using routine FAB mass spectrometry, ^1H and ^{19}F NMR spectroscopies and elemental analysis, among which complex **2b** was further identified using single crystal X-ray analysis to establish their exact solid state structure.

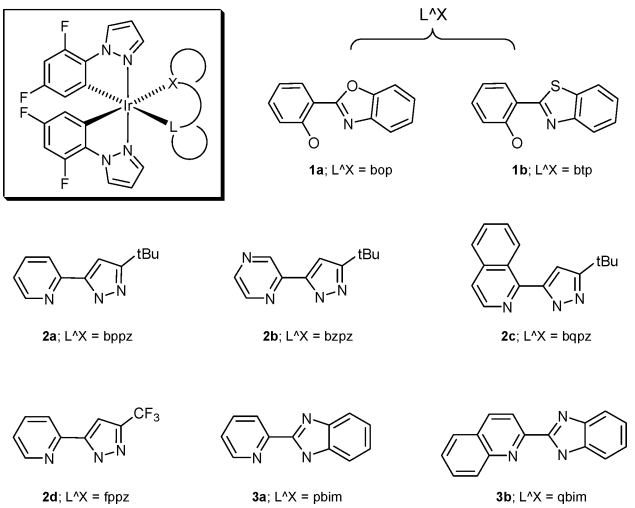

Chart 1

As depicted in Fig. 1, complex **2b** reveals a distorted octahedral geometry around the Ir atom with two cyclometalated dfpz ligands and one anionic 2-pyrazylpyrazolate (bzpzH) ligand. All three chelate ligands show small bite angles of 76.8–80.5°, which then induce minor structural distortion. The dfpz ligands adopt a mutually eclipsed configuration with the nitrogen atoms N(5) and N(7) residing at the *trans* locations, and the Ir–N distances lie between 1.998(4) and 2.005(4) Å. The cyclometalated carbon atoms C(12) and C(21) are mutually *cis* on the iridium and show marginally longer distances 2.007(4) and 2.004(5) Å. The third, anionic pzpz ligand displays notably elongated Ir–N distances of 2.143(4) and 2.102(4) Å *vs.* those of the *trans*-orientated Ir–N distances of the fppz ligands. Such an observation is believed to be caused by the stronger Ir–C bonding interaction of the dfpz ligands, which eventually weakens the Ir–N bonds at their *trans*-disposition. Moreover, the gross ligand arrangement is similar to several reported examples, including other cyclometalated Ir(III) complexes with pyridyl azolate serving as the ancillary ligand,[24] except that the Ir–N(pz) distance in **2b** (2.102(4) Å) is slightly longer than the Ir–N(pz) distance (2.096(3) Å) in the analogous CF_3 substituted complex **2d**,[25] this result being attributed to the electron donating *tert*-butyl group *vs.* the electron deficient CF_3 group in fppz ligand.

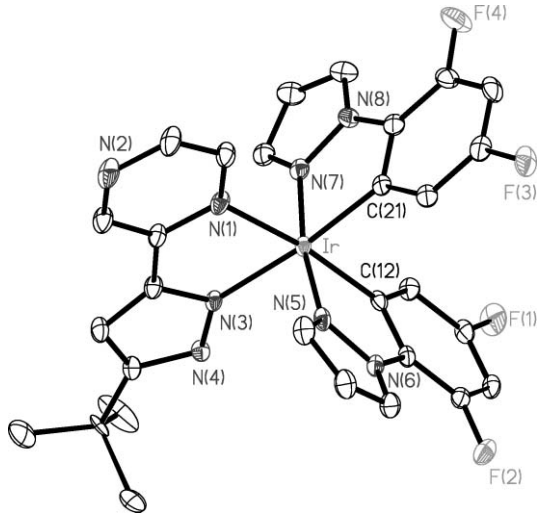

Fig. 1 ORTEP diagram of **2b** with thermal ellipsoids shown at 30% probability level; methyl groups of the *tert*-butyl substituent are disordered unequally over two orientations, only one of which is shown. Selected bond lengths (Å): Ir–N(1) = 2.143(4), Ir–N(3) = 2.102(4), Ir–N(5) = 1.998(4), Ir–N(7) = 2.005(4), Ir–C(12) = 2.007(4), Ir–C(21) = 2.004(5); bond angles (°): N(1)–Ir–N(3) = 76.8(1), N(5)–Ir–C(12) = 80.5(2), N(7)–Ir–C(21) = 80.4(2).

Photophysical data

The absorption and luminescence spectra were recorded for all samples in CH_2Cl_2. The numerical data are summarized in Table 2 and the associated spectra are depicted in Fig. 2. According to the structure of the chromophores, and hence the photophysical properties, the L^X ligands can be categorized into three classes, namely **1a–b**, **2a–d** and **3a–b**. As shown in Fig. 2a, the lowest energy absorption peaks of complexes **1a** and **1b** occurred in the region 416–441 nm (>5000 M^{-1} cm^{-1}), which can be ascribed to a typical spin-allowed $^1\pi\pi^*$ transition mixed with a small proportion of ^{1}MLCT transition. This hypothesis was confirmed by the observation of a similar spectral profile of the $\pi\pi^*$ transition maximized at 375 and 400 nm for the uncoordinated bop and btp anions, respectively. Concomitantly, the emission peaks of **1a** and **1b** occurred at λ_{max} = 522 and 574 nm, respectively, with a quantum efficiency of 0.82 for **1b** ($\tau \sim 7.6$ μs) being substantially greater than that of **1a** ($\Phi = 0.29$, $\tau \sim 10.7$ μs). The moderate separation of the 0–0 onsets between emission signal and the lowest energy absorption band, in combination with a broad spectral feature,

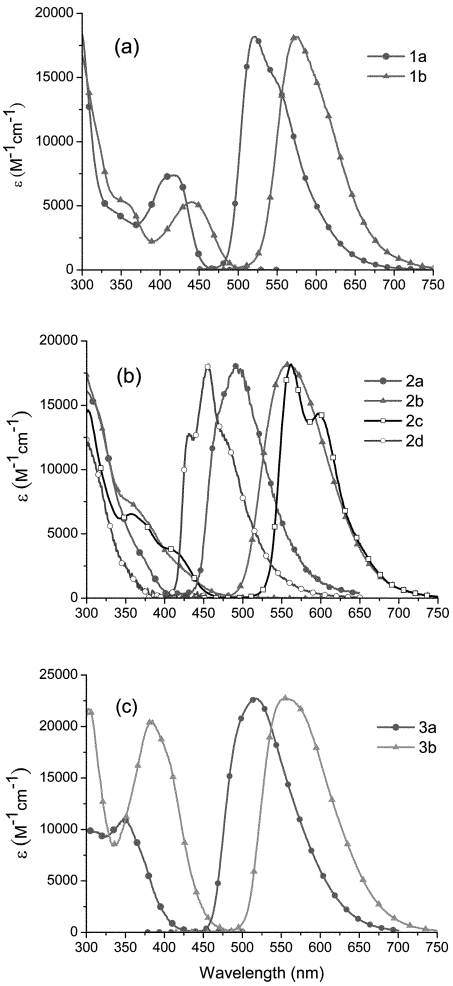

Fig. 2 UV/Vis absorption and emission spectra of complexes **1a** and **1b** (a), complexes **2a**–**2d** and complexes **3a** and **3b** (c) in CH_2Cl_2 at room temperature.

leads us to conclude that the phosphorescence originates primarily from the $^3\pi\pi$ state together, in part, with contribution from the ^{3}MLCT transition. The radiative lifetime of **1b** (9.3 μs), calculated using the equation $\tau_{rad} = \tau_{obs}/\Phi$, is also notably shorter than that of **1a** (36.9 μs), indicating an increased proportion of ^{3}MLCT character for the benzothiazolyl derivative **1b**. Qualitatively, this delineation is inconsistent with the diminished vibronic coupling

Table 2 Electrochemical data and photophysical properties of all iridium complexes[a]

Entry	λ_{abs}/nm ($\varepsilon \times 10^{-3}$/$M^{-1}$ cm^{-1})	λ_{em}/nm	Φ (%)	τ_{obs}/μs	τ_r/μs	$E_{1/2}^{ox}$/V (ΔE_p/mV)	$E_{1/2}^{red}$/V (ΔE_p/mV)
1a	345 (4.4), 416 (7.3)	522	29	10.7	36.9	0.55 (irr)	−2.03 (100)
1b	362 (4.9), 441 (5.3)	574	82	7.6	9.3	0.52 (irr)	−1.82 (120)
2a	272 (23.6), 302 (15.9), 346 (6.5), 374 (3.1)	490	6.0	0.79	13.2	0.72 (120)	−3.04 (irr)
2b	276 (21.2), 302 (16.9), 363 (7.0), 433 (1.7)	558	72.0	3.0	4.2	0.78 (100)	−2.27 (75)
2c	252 (24.1), 302 (14.6), 358 (6.4), 416 (3.3)	562, 596	100	20.2	20.2	0.72 (100)	−2.35 (90)
2d	267 (22.2), 290 (13.1), 349 (2.7), 372 (0.6)	440, 455, 478	0.67	0.042	6.3	0.98 (100)	−2.72 (irr)
3a	251 (23.2), 303 (9.9), 347 (10.9)	516	81	28.0	34.6	0.73 (irr)	−1.90 (110)
3b	255 (43.2), 303 (21.7), 385 (20.5)	555	80	14.7	18.4	0.71 (irr)	−1.53 (120)

[a] All photophysical data were recorded in degassed CH_2Cl_2 solution using three freeze–pump–thaw cycles. τ_{obs} and τ_r denote the observed and radiative decay time, respectively. $E_{1/2}$ refers to $[(E_{pa} + E_{pc})/2]$ where E_{pa} and E_{pc} are the anodic and cathodic peak potentials referenced to the Fc/Fc^+ couple. $\Delta E_p = |E_{pa} - E_{pc}|$ was reported in mV, and the oxidation and reduction experiments were conducted in CH_2Cl_2 and THF solution, respectively.

observed in the emission profile of **1b** (see Fig. 2a, *cf.* **1a**). Further support of this viewpoint is given by the electrochemical analyses (*vide infra*).

The absorption and emission spectra of the pyridylpyrazolate derivatives **2a**–**2d** are depicted in Fig. 2b. For **2a** and **2d**, the corresponding absorption spectra are characterized by an intense ligand localized ππ* transition in the UV region <400 nm, the results of which are consistent with the higher energy gap of all the chromophores, *i.e.* cyclometalated 1-(2,4-difluorophenyl)pyrazoles and pyridylpyrazolate ligands incorporated into their coordination sphere. In sharp contrast, both complexes **2b** and **2c** showed strong absorptions in the region >400 nm, which originated mainly from the spin-allowed ^{1}ππ* transitions of the bzpz and bqpz ligands. In comparison to **2a**, introducing an extra nitrogen atom forming pyrazine (in **2b**), or isoquinoline fragments to extend the π conjugation (in **2c**) lowered the gap of the S_0–S_1 transition. For the respective phosphorescence spectra, although complex **2d** exhibited the highest energy emission in the blue region (440–478 nm), its quantum yield turned out to be the lowest among this class of complexes. Such an observation can be attributed to the deliberate increase of the ligand energy gaps, for which the frontier orbitals attributed to the lowest triplet state may spread out to all ligated fragments possessing π chromophores, resulting in a mixing of various types of electronic transitions such as intraligand ππ* charge transfer (ILCT) and even ligand-to-ligand charge transfer (LLCT) transitions.[25,26] Further support of this viewpoint is given in the section of theoretical approaches. The net result is the weakening of all metal–ligand bonds, *i.e.* a possible loose molecular framework, giving rise to an enhanced radiationless deactivation process. Conversely, other complexes **2a**–**2c** displayed bright emission in the region 490–596 nm with substantially higher quantum efficiencies (see Table 2). For instance, complexes **2b** and **2c** exhibited an emission quantum efficiency as high as 72% and ~100%, respectively. Interestingly, however, despite a similar emission peak wavelength between **2b** and **2c**, the associated vibronic fine structures of the phosphorescence for **2c** suggests the emission originates primarily from the ^{3}ππ(ILCT) manifold, together with a somewhat reduced contribution from the ^{3}MLCT transition. This viewpoint is firmly supported by its substantially longer radiative lifetime (20.2 μs) relative to that of **2b** (4.2 μs, see Table 2).

Finally, as shown in Fig 2c, the third class of the benzimidazolate complexes **3a** and **3b** gave the lowest energy absorption band maxima at 347 and 385 nm and emission peak wavelength at 516 and 555 nm, respectively. Table 2 lists their respective photophysical data in solution phase at room temperature. The observed lifetimes of *ca.* 28 and 14.7 μs for **3a** and **3b**, together with the quantum yields of 0.81 and 0.80, respectively, in CH_2Cl_2, deduce a radiative lifetime of 34.6 for **3a** and 18.4 μs for **3b**. The short radiative lifetime, in combination with relatively broad, structureless phosphorescence, manifests a typical transition incorporating ^{3}ππ*/^{3}MLCT mixing character. In comparison to **3a** with a pyridyl group at the benzimidazolate chelate, complex **3b** bearing a 2-quinolinyl group reveals an ~40 nm bathochromic shift in the emission wavelength, the result of which can be promptly rationalized by a decrease of the LUMO energy level resulting from the increase of π-conjugation in the 2-quinolinyl group (*versus* the pyridyl moiety in **3a**).

Theoretical approaches

Further insights into the photophysical properties of these complexes are gained from a theoretical approach (TD-B3LYP/6-31G* and LANL2DZ//B3LYP/6-31G* and LANL2DZ, see Experimental section). For some representative complexes, the features of the frontier orbitals mainly involved in the electronic transitions are depicted in Fig. 3, while the descriptions and the energy gap of each transition are listed in Table 3. As listed in Table 3, for complexes **1a**–**3b**, the lowest singlet (S_1) and triplet (T_1) states are mainly contributed to from the HOMO → LUMO transition. In addition, the calculated excitation energies for the lowest singlet (S_1) and triplet (T_1) states are in very good agreement with the measured absorption and emission energies, respectively. We thus believed that the theoretical level adopted here is suitable for interpreting the photophysical properties of the studied Ir(III) complexes in a qualitative manner.

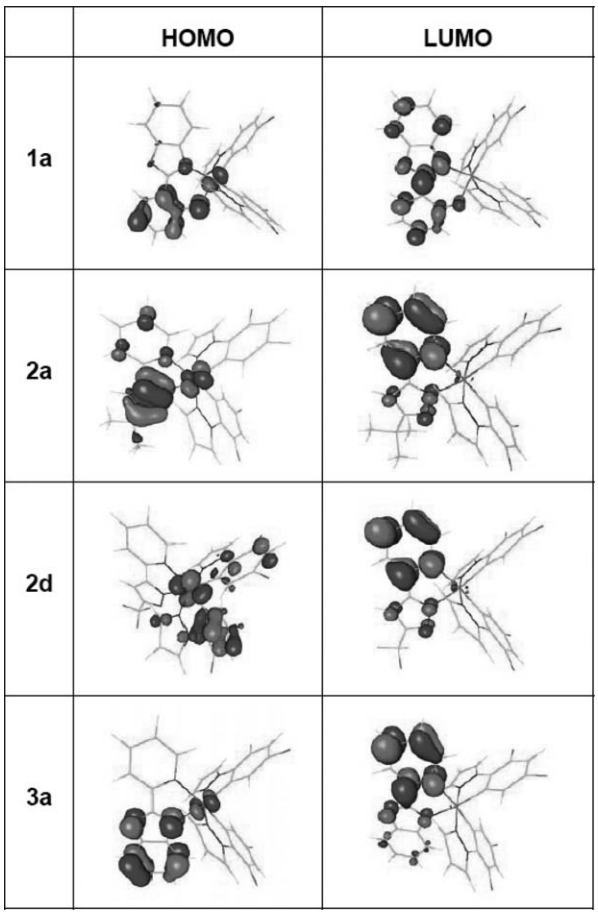

Fig. 3 Selected frontier orbitals of representative complexes **1a**, **2a**, **2d** and **3a**.

Complexes **1a** and **1b** (not shown here) reveal a similar frontier orbital configuration. The transitions for the lowest-lying excited states (S_1 and T_1) are mainly contributed to the intra-ligand ππ* charge transfer, that is, shifting from the phenolate to the benzoxazolyl (**1a**) (or benzothiazolyl in **1b**) moieties, accompanied by the Ir(d_π) → π* (benzoxazolyl in **1a**, or benzothiazolyl in **1b**) MLCT. Consistent with the experimental results, the calculated S_0–S_1 enegy gap of **1b** is red shifted by as much as ~2400 cm^{-1} with

Table 3 Calculated energy levels of the lower lying transitions of complexes **1a**–**3b**

		Assignment	λ/nm	f
1a	S_1	HOMO → LUMO (+85%)	412.3	0.1249
	T_1	HOMO → LUMO (+108%)	536.7	~0
1b	S_1	HOMO → LUMO (+86%)	457.7	0.0744
	T_1	HOMO → LUMO (+106%)	580.4	~0
2a	S_1	HOMO → LUMO (+88%)	374.2	0.0308
	T_1	HOMO → LUMO (+80%)	457.9	~0
		HOMO − 2 → LUMO (+18%)		
		HOMO → LUMO + 2 (+9%)		
2b	S_1	HOMO → LUMO (+88%)	421.1	0.0203
	T_1	HOMO → LUMO (+87%)	518.2	~0
		HOMO − 2 → LUMO (21%)		
2c	S_1	HOMO → LUMO (+80%)	423.8	0.0776
		HOMO − 2 → LUMO (+9%)		
	T_1	HOMO → LUMO (+90%)	562.8	~0
		HOMO − 2 → LUMO (+20%)		
2d	S_1	HOMO → LUMO (+81%)	365.8	0.0209
	T_1	HOMO → LUMO (+65%)	424.2	~0
		HOMO − 1 → LUMO (+23%)		
3[a]	S_1	HOMO → LUMO (+90%)	406.5	0.0206
	T_1	HOMO → LUMO (+75%)	503.3	~0
		HOMO − 1 → LUMO (+23%)		
3b	S_1	HOMO → LUMO (+91%)	458.8	0.0130
	T_1	HOMO → LUMO (+64%)	551.0	~0
		HOMO − 1 → LUMO (+37%)		
		HOMO → LUMO+3 (+6%)		

respect to that of **1a**. The result may be rationalized by the fact that the sulfur atom (benzothiazolyl moiety in **1b**) is more polarizable than the oxygen atom (benzoxazolyl moiety in **1a**), resulting in an increase of the conjugative effect and hence a smaller ππ* energy gap. Similar frontier-orbital configurations were found among **2a**–**2c** (**2b** and **2c** not shown here). The electron densities of the HOMO are mainly located on the central Ir metal atom and the pyrazolate fragment of the bidentate ancillary ligand (L^X), while those of the LUMO are primarily distributed over another moiety of the same ligand. The results clearly indicate that the lowest-lying singlet (S_1) and triplet states (T_1) are composed of MLCT in combination with a ππ* transition (ILCT) in character. In sharp contrast, for complex **2d**, only a small portion of electron density in the HOMO locates at the pyrazolate fragment. Instead, it is mainly distributed on the difluorophenyl moieties. The result can be rationalized by the addition of a strong electron withdrawing group, *i.e.* CF_3, in the pyrazolate fragment, resulting in a significant decrease of the π orbital energy in the pyrazolate moiety, which no longer serves as a major contribution to the HOMO in **2d**. The switch of transition from ILCT (**2a**–**2c**) to LLCT (**2d**) should lead to the spreading of electron densities over the molecular framework and hence a possible looser structure (*vice supra*) that induces an efficient radiationless transition, consistent with the lowest emission quantum efficieny for **2a** among complexes **2a**–**2d**.

Also depicted in Fig. 3, the lowest lying states (S_1 and T_1) for both **3a** and **3b** (not shown here) can be described as a typical MLCT mixed with π (benzoimidazolate) → π* (pyridyl in **3a**, 2-quinolinyl in **3b**) ILCT. Apparently, the replacement of pyridyl (**3a**) by the 2-quinolinyl group (**3b**) leads to a decrease of the LUMO energy level due to the increase of π-conjugation in the 2-quinolinyl group (*versus* the pyridyl moiety in **3a**). As a result, in comparison to **3a**, the ~40 nm bathochromic shift in the emission wavelength of **3b** can be fully justified.

Electrochemistry

The electrochemical behavior of these iridium complexes was investigated using cyclic voltammetry; the data are also listed in Table 2. It is notable that the oxidation potential of complexes **1a** and **1b** (0.52–0.55 V) is significantly lower than those of the pyrazolate complexes **2a**–**2d** (0.72–0.98 V) and imidazolate complexes **3a**–**3b** with potentials spanning the 0.71–0.73 V range. As revealed by previous electrochemical studies[27] and theoretical calculations,[8] the one-electron oxidation of such d^6 complexes would mainly occur at the metal site, together with a minor contribution from the surrounding chelates. Thus, the lowered oxidation potential of **1a** and **1b** is attributed to the phenolate ligand, which destabilized the metal d orbitals *via* donation of the lone pair of the oxygen atom. Furthermore, in comparison to that of **1a** (0.55 V), the lower oxidation potential in **1b** (0.52 V) may imply a lift of the d_π orbital, rationalizing its greater ^{3}MLCT contribution (*vide supra*). Conversely, complexes **2a**–**2d** and **3a**–**3b** possess only the pyrazolate or the imidazolate ligands, in which no lone pair donation is available; thus the oxidation potentials are relatively higher than those of the complexes **1a** and **1b**.

Upon switching to the reduction sweep in THF, one reversible, lower energy reduction process was detected for all of them, except for the complexes **2a** and **2d**, which turned out to be irreversible. These data are in good agreement with the greatest blue shift for their emission signals, showing the possession of the highest destabilized LUMO among all complexes. Moreover, the reduction potentials of iridium complexes within each subgroup also showed good correlation with the nature of the third, ancillary L^X ligand. For instance, substitution of the bop ligand in **1a** by the more electron donating btp ligand in **1b** markedly decreased the reduction potential (−2.03 to −1.82 V) as well as the oxidative potential (0.55 to 0.52 V). It should be noted that the variation in the reduction potentials was much greater than the difference observed for the oxidation potentials. This result firmly supports the original concept that the reduction mainly occurred at the ancillary L^X ligand. In view of the oxidation potentials, comparing the same class of L^X ligands such as **2a**–**2d** and **3a**–**3b**, except for **2d**, the smaller variation in oxidation potential was due to a less pronounced inductive effect that transmitted to the central metal atom, confirming that both reduction and oxidation reactions mainly occurred at the L^X ligand and the adjacent iridium metal site, respectively. Conversely, the significantly higher oxidation potential (0.98 V, see Table 2) in **2d** manifests its different type of ligand contribution to the HOMO, *i.e.* the difluorophenyl rather than the pyrazolate moiety in **2d** concluded from the theoretical approach.

Electroluminescent devices

To demonstrate their capabilities in exhibiting decent electroluminescent properties, complex **2b** was selected as the representative example as it exhibited a relatively shorter radiative lifetime in solution. It should be noted that, despite its unit emission quantum efficiency, **2c** was not picked as a prototype simply due to its relatively much longer radiative lifetime (*vide*

Table 4 Performance characteristics for ITO/NPB/CBP : *x* wt% **2b**/BCP/AlQ_3/Mg : Ag devices

x conc. (%)	Max. lum.[a]/cd m^{-2}	Quantum efficiency[b] (%)	Luminous efficiency[b]/cd A^{-1}	Power efficiency[b]/lm W^{-1}	λ_{max}/nm (C.I.E. coordinates[c])
7%	60 036 (14.5)	6.11 (5.03)	23.2 (19.1)	9.6 (6.3)	526 (0.34, 0.61)
14%	33 865 (16.0)	6.05 (4.56)	22.8 (17.3)	7.7 (4.6)	528 (0.32, 0.62)
28%	33 760 (16.0)	5.69 (4.10)	21.2 (15.1)	7.1 (4.1)	530 (0.33, 0.61)
50%	10 298 (14.5)	2.01 (1.48)	7.5 (5.5)	2.4 (1.5)	536 (0.32, 0.62)
100%	15 485 (16.0)	2.21 (1.82)	8.1 (6.7)	2.2 (1.5)	536 (0.37, 0.58)

[a] Values in the parentheses are the applied driving voltage (in V). [b] Data collected at 20 mA cm^{-2}, while values in parentheses are the data collected at 100 mA cm^{-2}. [c] Measured at the driving voltage of 9 V.

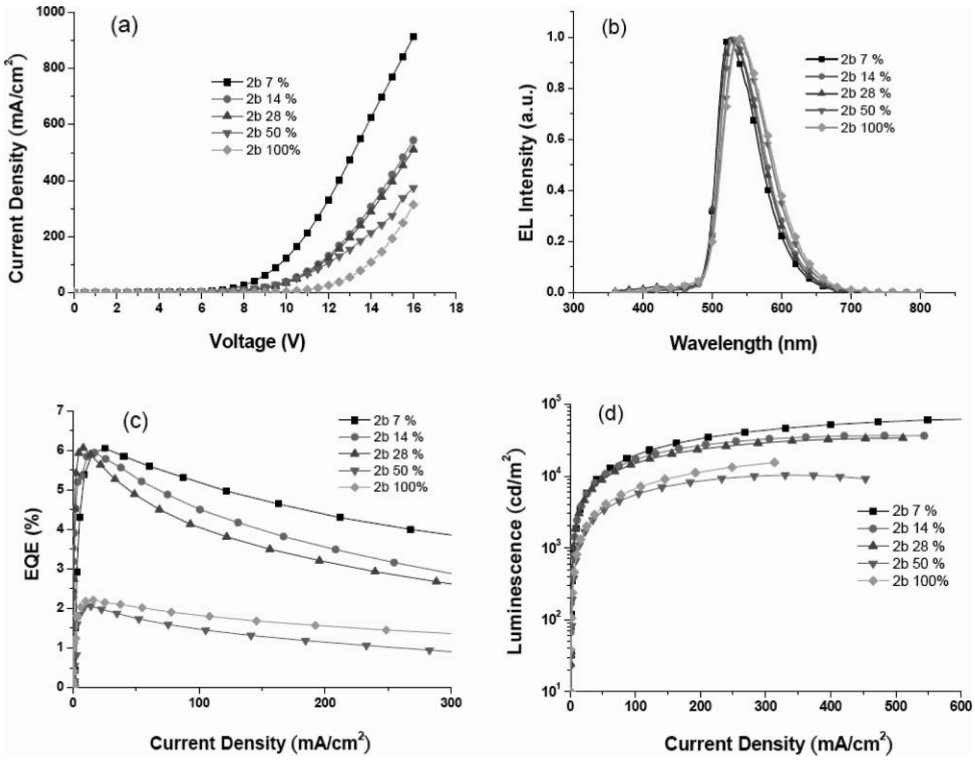

Fig. 4 (a) Current density *vs*. applied voltage for the **2b**-doped devices, (b) EL spectra of all devices, (c) external quantum efficiency *vs*. current density, and (d) luminescence *vs*. current density.

supra). The devices incorporating **2b** are prepared using thermal evaporation and their structures consist of the multilayer configuration ITO/NPB (40 nm)/CBP : *x* wt% of **2b** (30 nm)/BCP (10 nm)/AlQ_3(30 nm)/Mg : Ag (100 nm), where NPB, CBP, BCP and AlQ_3 stand for 1,4-bis(1-naphthylphenylamino)biphenyl, 4,4′-*N*.*N*′-dicarbazolyl-1,1′-biphenyl, 2,9-dimethyl-4,7-diphenyl-1,10-phenanthroline, and tris(8-hydroxyquinolinato)aluminium(III) respectively; whilst the BCP layer acts as a hole blocker to prevent any emission from AlQ_3. The crucial device performance characteristics are collected in Table 4, showing the systematic trend that varied according to the five dopant concentrations from 7% to 100%. Bright greenish yellow emission was observed for all the concentrations applied, even for the one with a pure layer of the Ir(III) emitter. Fig. 4a shows the current–voltage curves of the electroluminescent devices for **2b** at various doping concentrations. The driving voltages of these devices increase with dopant concentrations, consistent with earlier reports that iridium complexes behave as carrier traps in devices.[28] Concomitantly, a small red shifting of the EL emission was observed with increasing dopant concentrations, *e.g.* from λ_{max} = 526 nm for the 7% device to 536 nm for the device with neat dopant (Fig. 4b). This effect is presumably attributed to the change of the medium polarity.[29]

Among various dopant concentration, the best device performance was achieved at 7 wt% (Fig. 4c), which rendered a turn-on voltage of 4 V (at 1 cd m^{-2}) and peak EQE of 6.11 at 5.03 V, reached the maximum brightness of 60 036 cd m^{-2} at a driving voltage of 14.5 V and with C.I.E. coordinates of 0.34, 0.61 at 9 V. Like other phosphorescent emitters, the efficiencies also witnessed a drop with increasing driving voltage.[30] At a driving current of 20 mA cm^{-2}, the external quantum efficiency is 6.11% and luminous efficiency is 23.19 cd A^{-1}, whereas at 100 mA cm^{-2} the efficiencies remain at 5.03% and 19.09 cd A^{-1} respectively. However, this efficiency roll-off at high current densities is much less pronounced than those reported for the triplet-state emitters.[31] The key difference is plausibly due to the short radiative lifetime of complex **2b**, which significantly reduces the triplet–triplet annihilation.[15,32]

As a result of concentration quenching, raising the doping concentration leads to a fall off in device efficiency.[33] Relatively

bright luminescence of over 10 000 cd m^{-2} was observed for other concentrations applied (≤28%), albeit with significant decrease of intensity once the concentration was increased over 28% (Fig. 4d), which is evidence of the device using 50% of **2b** as dopant, showing the peak EQE of 2.01 at 1.48 V, maximum brightness of 10 298 cd m^{-2} at a driving voltage of 14.5 V and with C.I.E. coordinates of 0.32, 0.62 at 9 V. Upon further increasing of the dopant concentration to 100%, the device exhibits a comparable peak EQE of 2.21 at 1.82 V, while the maximum brightness is lowered to 15485 cd/m^2 at 16.0 V and showing C.I.E. coordinates of (0.37, 0.58) at 9 V.

Conclusions

In summary, we report the preparation of a series of new heteroleptic Ir(III) metal complexes chelated by two cyclometalated 1-(2,4-difluorophenyl)pyrazole ligands (dfpz)H and a third ancillary bidantate ligand (L^X). This intricate design lies in a core concept that the cyclometalated dfpz ligands ensure a greater ππ* gap in these series of iridium complexes. Accordingly, the lowest one-electron excitation would accommodate the π* orbital of the ancillary L^X ligands. The experimental results firmly support the original concept in that reduction mainly occurred at the ancillary L^X ligand; whereas the smaller variation of oxidation potential was due to a less pronounced inductive effect that transmitted to the central metal atom. Except for **2d**, the redox potentials of the entire series of complexes are consistent with the delineation that the reduction and oxidation reactions mainly occurr at the L^X ligand and the adjacent iridium metal site, respectively. The feasibility of OLED application is given by complex **2b**, which was used as a representative example for fabrication of the multilayered, green-emitting phosphorescent OLEDs using direct thermal evaporation techniques. From the viewpoint of strategic design, this series of heteroleptic cyclometalated Ir(III) complexes establish a simple and straightforward methodology for color tuning *via* incorporation of the facile variation of ancillary ligands only.

Notes and references

1 (*a*) E. Holder, B. M. W. Langeveld and U. S. Schubert, *Adv. Mater.*, 2005, **17**, 1109; (*b*) P.-T. Chou and Y. Chi, *Eur. J. Inorg. Chem.*, 2006, 3319; (*c*) H. Yersin, *Top. Curr. Chem.*, 2004, **241**, 1; (*d*) R. C. Evans, P. Douglas and C. J. Winscom, *Coord. Chem. Rev.*, 2006, **250**, 2093; (*e*) Y. Chi and P.-T. Chou, *Chem. Soc. Rev.*, 2007, 36, DOI: 10.1039/b608951h.

2 (*a*) C. Adachi, M. A. Baldo, M. E. Thompson and S. R. Forrest, *J. Appl. Phys.*, 2001, **90**, 5048; (*b*) S. Tokito, T. Iijima, T. Tsuzuki and F. Sato, *Appl. Phys. Lett.*, 2003, **83**, 2459; (*c*) S.-C. Lo, E. B. Namdas, P. L. Burn and I. D. W. Samuel, *Macromolecules*, 2003, **36**, 9721; (*d*) G. He, S.-C. Chang, F.-C. Chen, Y. Li and Y. Yang, *Appl. Phys. Lett.*, 2002, **81**, 1509; (*e*) C.-L. Lee, K. B. Lee and J.-J. Kim, *Appl. Phys. Lett.*, 2000, **77**, 2280.

3 (*a*) V. V. Grushin, N. Herron, D. D. LeCloux, W. J. Marshall, V. A. Petrov and Y. Wang, *Chem. Commun.*, 2001, 1494; (*b*) Y. You and S. Y. Park, *J. Am. Chem. Soc.*, 2005, **127**, 12438.

4 (*a*) Z. He, W.-Y. Wong, X.-M. Yu, H.-S. Kwok and Z.-Y. Lin, *Inorg. Chem.*, 2006, **45**, 10922; (*b*) W. Lu, B.-X. Mi, M. C. W. Chan, Z. Hui, C.-M. Che, N. Zhu and S.-T. Lee, *J. Am. Chem. Soc.*, 2004, **126**, 4958.

5 (*a*) S.-Y. Chang, J. Kavitha, S.-W. Li, C.-S. Hsu, Y. Chi, Y.-S. Yeh, P.-T. Chou, G.-H. Lee, A. J. Carty, Y.-T. Tao and C.-H. Chien, *Inorg. Chem.*, 2006, **45**, 137; (*b*) J. Kavitha, S.-Y. Chang, Y. Chi, J.-K. Yu, Y.-H. Hu, P.-T. Chou, S.-M. Peng, G.-H. Lee, Y.-T. Tao, C.-H. Chien and A. J. Carty, *Adv. Funct. Mater.*, 2005, **15**, 223.

6 (*a*) P.-T. Chou and Y. Chi, *Chem.–Eur. J.*, 2007, **13**, 380; (*b*) F.-C. Hsu, Y.-L. Tung, Y. Chi, C.-C. Hsu, Y.-M. Cheng, M.-L. Ho, P.-T. Chou, S.-M Peng and A. J. Carty, *Inorg. Chem.*, 2006, **45**, 10188; (*c*) Y.-L. Tung, S.-W. Lee, Y. Chi, Y.-T. Tao, C.-H. Chien, Y.-M. Cheng, P.-T. Chou, S.-M. Peng and C.-S. Liu, *J. Mater. Chem.*, 2005, **15**, 460; (*d*) Y.-L. Tung, P.-C. Wu, C.-S. Liu, Y. Chi, J.-K. Yu, Y.-H. Hu, P.-T. Chou, S.-M. Peng, G.-H. Lee, Y. Tao, A. J. Carty, C.-F. Shu and F.-I. Wu, *Organometallics*, 2004, **23**, 3745; (*e*) P.-C. Wu, J.-K. Yu, Y.-H. Song, Y. Chi, P.-T. Chou, S.-M. Peng and G.-H. Lee, *Organometallics*, 2003, **22**, 4938; (*f*) K. Chen, Y.-M. Cheng, Y. Chi, M.-L. Ho, C.-H. Lai, P.-T. Chou, S.-M. Peng and G.-H. Lee, *Chem.–Asian J.*, 2007, **2**, 155.

7 (*a*) W.-Y. Wong, G.-J. Zhou, X.-M. Yu, H.-S. Kwok and B.-Z. Tang, *Adv. Funct. Mater.*, 2006, **16**, 838; (*b*) Z. Liu, M. Guan, Z. Bian, D. Nie, Z. Gong, Z. Li and C. Huang, *Adv. Funct. Mater.*, 2006, **16**, 1441; (*c*) C.-H. Yang, W.-L. Su, K.-H. Fang, S.-P. Wang and I.-W. Sun, *Organometallics*, 2006, **25**, 4514; (*d*) G.-J. Zhou, W.-Y. Wong, B. Yao, Z.-Y. Xie and L.-I. Wang, *Angew. Chem., Int. Ed.*, 2007, **46**, 1149; (*e*) W.-Y. Wong, C.-L. Ho, Z.-Q. Gao, B.-X. Mi, C.-H. Chen, K.-W. Cheah and Z.-Y. Lin, *Angew. Chem., Int. Ed.*, 2006, **45**, 7800; (*f*) W.-Y. Wong, G.-J. Zhou, X.-M. Yu, H.-S. Kwok and Z.-Y. Lin, *Adv. Funct. Mater.*, 2007, **17**, 315.

8 (*a*) P. J. Hay, *J. Phys. Chem. A*, 2002, **106**, 1634; (*b*) S. Jung, Y. Kang, H.-S. Kim, Y.-H. Kim, C.-L. Lee, J.-J. Kim, S.-K. Lee and S.-K. Kwon, *Eur. J. Inorg. Chem.*, 2004, 3415.

9 (*a*) R. Ragni, E. A. Plummer, K. Brunner, J. W. Hofstraat, F. Babudri, G. M. Farinola, F. Naso and L. De Cola, *J. Mater. Chem.*, 2006, **16**, 1161; (*b*) X. Zhang, J. Gao, C. Yang, L. Zhu, Z. Li, K. Zhang, J. Qin, H. You and D. Ma, *J. Organomet. Chem.*, 2006, **691**, 4312.

10 (*a*) J. Li, P. I. Djurovich, B. D. Alleyne, M. Yousufuddin, N. N. Ho, J. C. Thomas, J. C. Peters, R. Bau and M. E. Thompson, *Inorg. Chem.*, 2005, **44**, 1713; (*b*) S. Lamansky, P. Djurovich, D. Murphy, F. Abdel-Razzaq, R. Kwong, I. Tsyba, M. Bortz, B. Mui, R. Bau and M. E. Thompson, *Inorg. Chem.*, 2001, **40**, 1704; (*c*) Q. Zhao, C.-Y. Jiang, M. Shi, F.-Y. Li, T. Yi, Y. Cao and C.-H. Huang, *Organometallics*, 2006, **25**, 3631.

11 (*a*) M. K. Nazeeruddin, R. Humphry-Baker, D. Berner, S. Rivier, L. Zuppiroli and M. Graetzel, *J. Am. Chem. Soc.*, 2003, **125**, 8790; (*b*) F.-M. Hwang, H.-Y. Chen, P.-S. Chen, C.-S. Liu, Y. Chi, C.-F. Shu, F.-I. Wu, P.-T. Chou, S.-M. Peng and G.-H. Lee, *Inorg. Chem.*, 2005, **44**, 1344; (*c*) L. Chen, H. You, C. Yang, D. Ma and J. Qin, *Chem. Commun.*, 2007, DOI: 10.1039/b616493e.

12 (*a*) A. Tsuboyama, H. Iwawaki, M. Furugori, T. Mukaide, J. Kamatani, S. Igawa, T. Moriyama, S. Miura, T. Takiguchi, S. Okada, M. Hoshino and K. Ueno, *J. Am. Chem. Soc.*, 2003, **125**, 12971; (*b*) S. Okada, K. Okinaka, H. Iwawaki, M. Furugori, M. Hashimoto, T. Mukaide, J. Kamatani, S. Igawa, A. Tsuboyama, T. Takiguchi and K. Ueno, *Dalton Trans.*, 2005, 1583.

13 A. B. Tamayo, B. D. Alleyne, P. I. Djurovich, S. Lamansky, I. Tsyba, N. N. Ho, R. Bau and M. E. Thompson, *J. Am. Chem. Soc.*, 2003, **125**, 7377.

14 A. B. Tamayo, S. Garon, T. Sajoto, P. I. Djurovich, I. M. Tsyba, R. Bau and M. E. Thompson, *Inorg. Chem.*, 2005, **44**, 8723.

15 T.-H. Kwon, H. S. Cho, M. K. Kim, J.-W. Kim, J.-J. Kim, K. H. Lee, S. J. Park, I.-S. Shin, H. Kim, D. M. Shin, Y. K. Chung and J.-I. Hong, *Organometallics*, 2005, **24**, 1578.

16 C.-C. Cheng, W.-S. Yu, P.-T. Chou, S.-M. Peng, G.-H. Lee, P.-C. Wu, Y.-H. Song and Y. Chi, *Chem. Commun.*, 2003, 2628.

17 I. L. Finar and D. M. Rackham, *J. Chem. Soc. B*, 1968, 211.

18 F. Gumus, I. Pamuk, T. Ozden, S. Yildiz, N. Diril, E. Oksuzoglu, S. Gur and A. Ozkul, *J. Inorg. Biochem.*, 2003, **94**, 255.

19 J. N. Demas and G. A. Crosby, *J. Phys. Chem.*, 1971, **75**, 991.

20 J. M. Drake, M. L. Lesiecki and D.M. Camaioni, *Chem. Phys. Lett.*, 1985, **113**, 530.

21 (*a*) C. Lee, W. Yang and R. G. Parr, *Phys. Rev. B*, 1988, **37**, 785; (*b*) A. D. Becke, *J. Chem. Phys.*, 1993, **98**, 5648.

22 (*a*) P. J. Hay and W. R. Wadt, *J. Chem. Phys.*, 1985, **82**, 270; (*b*) W. R. Wadt and P. J. Hay, *J. Chem. Phys.*, 1985, **82**, 284; (*c*) P. J. Hay and W. R. Wadt, *J. Chem. Phys.*, 1985, **82**, 299.

23 M. J. Frisch, G. W. Trucks, H. B. Schlegel, G. E. Scuseria, M. A. Robb, J. R. Cheeseman, J. A. Montgomery, Jr., T. Vreven, K. N. Kudin, J. C. Burant, J. M. Millam, S. S. Iyengar, J. Tomasi, V. Barone, B. Mennucci, M. Cossi, G. Scalmani, N. Rega, G. A. Petersson, H. Nakatsuji, M. Hada, M. Ehara, K. Toyota, R. Fukuda, J. Hasegawa, M. Ishida, T. Nakajima, Y. Honda, O. Kitao, H. Nakai, M. Klene, X. Li, J. E. Knox, H. P. Hratchian, J. B. Cross, V. Bakken, C. Adamo, J. Jaramillo, R. Gomperts, R. E. Stratmann, O. Yazyev, A. J. Austin, R. Cammi, C. Pomelli, J. W. Ochterski, P. Y. Ayala, K. Morokuma, G. A. Voth, P. Salvador, J. J. Dannenberg, V. G. Zakrzewski, S. Dapprich, A. D. Daniels, M. C. Strain, O. Farkas, D. K. Malick, A. D. Rabuck, K.

Raghavachari, J. B. Foresman, J. V. Ortiz, Q. Cui, A. G. Baboul, S. Clifford, J. Cioslowski, B. B. Stefanov, G. Liu, A. Liashenko, P. Piskorz, I. Komaromi, R. L. Martin, D. J. Fox, T. Keith, M. A. Al-Laham, C. Y. Peng, A. Nanayakkara, M. Challacombe, P. M. W. Gill, B. Johnson, W. Chen, M. W. Wong, C. Gonzalez and J. A. Pople, *Gaussian 03, Revision C.03*, Gaussian, Inc., Wallingford, CT, 2004.

24 Y.-H. Song, S.-J. Yeh, C.-T. Chen, Y. Chi, C.-S. Liu, J.-K. Yu, Y.-H. Hu, P.-T. Chou, S.-M. Peng and G.-H. Lee, *Adv. Funct. Mater.*, 2004, **14**, 1221.

25 C.-H. Yang, S.-W. Li, Y. Chi, Y.-M. Cheng, Y.-S. Yeh, P.-T. Chou, G.-H. Lee, C.-H. Wang and C.-F. Shu, *Inorg. Chem.*, 2005, **44**, 7770.

26 Y.-S. Yeh, Y.-M. Cheng, P.-T. Chou, G.-H. Lee, C.-H. Yang, Y. Chi and C.-H. Wang, *ChemPhysChem*, 2006, **7**, 2294.

27 (*a*) Y. Ohsawa, S. Sprouse, K. A. King, M. K. DeArmond, K. W. Hanck and R. J. Watts, *J. Phys. Chem.*, 1987, **91**, 1047; (*b*) T. Yutaka, S. Obara, S. Ogawa, K. Nozaki, N. Ikeda, T. Ohno, Y. Ishii, K. Sakai and M. Haga, *Inorg. Chem.*, 2005, **44**, 4737.

28 X. Gong, J. C. Ostrowski, D. Moses, G. C. Bazan and A. J. Heeger, *Adv. Funct. Mater.*, 2003, **13**, 439.

29 V. Bulovic, R. Deshpande, M. E. Thompson and S. R. Forrest, *Chem. Phys. Lett.*, 1999, **308**, 317.

30 (*a*) Y.-L. Tung, L.-S. Chen, Y. Chi, P.-T. Chou, Y.-M. Cheng, E. Y. Li, G.-H. Lee, C.-F. Shu, F.-I. Wu and A. J. Carty, *Adv. Funct. Mater.*, 2006, **16**, 1615; (*b*) Y.-L. Tung, S.-W. Lee, Y. Chi, L.-S. Chen, C.-F. Shu, F.-I. Wu, A. J. Carty, P.-T. Chou, S.-M. Peng and G.-H. Lee, *Adv. Mater.*, 2005, **17**, 1059.

31 (*a*) C. Adachi, M. A. Baldo, S. R. Forrest, S. Lamansky, M. E. Thompson and P. C. Kwong, *Appl. Phys. Lett.*, 2001, **78**, 1622; (*b*) F.-C. Chen, Y. Yang, M. E. Thompson and J. Kido, *Appl. Phys. Lett.*, 2002, **80**, 2308.

32 M. A. Baldo, C. Adachi and S. R. Forrest, *Phys. Rev. B*, 2000, **62**, 10967.

33 M. A. Baldo, D. F. O'Brien, Y. You, A. Shoustikov, S. Sibley, M. E. Thompson and S. R. Forrest, *Nature*, 1998, **395**, 151.

